

Increased forest ecosystem carbon and nitrogen storage from nitrogen rich bedrock

Scott L. Morford¹, Benjamin Z. Houlton¹ & Randy A. Dahlgren¹

Nitrogen (N) limits the productivity of many ecosystems worldwide, thereby restricting the ability of terrestrial ecosystems to offset the effects of rising atmospheric CO₂ emissions naturally^{1,2}. Understanding input pathways of bioavailable N is therefore paramount for predicting carbon (C) storage on land, particularly in temperate and boreal forests^{3,4}. Paradigms of nutrient cycling and limitation posit that new N enters terrestrial ecosystems solely from the atmosphere. Here we show that bedrock comprises a hitherto overlooked source of ecologically available N to forests. We report that the N content of soils and forest foliage on N-rich metasedimentary rocks (350–950 mg N kg⁻¹) is elevated by more than 50% compared with similar temperate forest sites underlain by N-poor igneous parent material (30–70 mg N kg⁻¹). Natural abundance N isotopes attribute this difference to rock-derived N: ¹⁵N/¹⁴N values for rock, soils and plants are indistinguishable in sites underlain by N-rich lithology, in marked contrast to sites on N-poor substrates. Furthermore, forests associated with N-rich parent material contain on average 42% more carbon in above-ground tree biomass and 60% more carbon in the upper 30 cm of the soil than similar sites underlain by N-poor rocks. Our results raise the possibility that bedrock N input may represent an important and overlooked component of ecosystem N and C cycling elsewhere.

Globally, sedimentary rocks contain 10²¹ g of fixed N, considerably more than the 10¹⁹ g of fixed N in the total biosphere⁵. Such N is primarily derived from the burial of organic matter in marine and freshwater sediments, where it is incorporated into rock as organic N or as ammonium in silicate minerals. Sedimentary and metasedimentary rocks are distributed globally and typically contain between 200 and 1,200 mg N kg⁻¹, whereas high-grade metamorphic and igneous rocks typically contain less than 40 mg N kg⁻¹ (ref. 6). Fixed N is also found as nitrate salts in arid environments⁷, owing to the deposition of atmospheric N over millennia.

Reservoirs of silicate N were identified more than half a century ago⁸, but it is generally believed that rock N is not sufficiently important to alter the terrestrial N cycle, despite evidence to the contrary⁹. Just as weathering of phosphorus (P) from bedrock is considered the dominant source of P to terrestrial ecosystems¹⁰, geological N may also be a long-term source of bioavailable N to plants and ecosystems. Bedrock has already been implicated as a source of N to aquifers¹¹ and surface waters¹². Here we show, using a range of chemical and isotopic techniques, that bedrock contributes substantial amounts of N to temperate coniferous forests. In addition, we conducted a regional-scale investigation of 88 forest inventory and analysis (FIA) plots to show that total forest carbon storage is higher in ecosystems underlain by N-rich bedrock than in those underlain by N-poor rocks.

We tested the hypothesis that rock weathering is an ecologically significant N source that can increase forest productivity and C storage in temperate coniferous forests of northern California, USA. The first site, South Fork Mountain (SFM), is underlain by mica schist derived from low-grade metamorphism of marine sediments dating to the early Cretaceous period¹³. The mica phase of the schist contains at least 2,700 mg N kg⁻¹ as interlayer ammonium that is released to soil

solution as the rock weathers¹⁴. Our second site, adjacent to SFM, is underlain by the Bear Wallow Diorite Complex (BWDC), a plutonic rock dating to the Jurassic period¹³.

These sites have common tectonic histories, with significant uplift initiated during the Pleistocene¹⁵ and modern uplift rates estimated to be from 1 to 4 mm yr⁻¹ (see Methods). Other than parent material, all other state factors are similar across sites (Table 1). Soils at both sites are classified as Dystrochrepts, have sandy loam to loam texture, and show soil development to a depth of 0.5–1.0 m. The strontium isotope (⁸⁷Sr/⁸⁶Sr) composition of foliage from SFM and BWDC suggests that the two sites receive similar fractions of Sr inputs from precipitation and bedrock (Supplementary Fig. 1). Although differences in mineralogy and Sr concentration preclude a direct comparison of bedrock weathering inputs between sites¹⁶, the foliar Sr data are consistent with other soil metrics in suggesting that the weathering status of our sites is comparable. In addition, stand composition and tree age at SFM (tree age 121 ± 7.5 years, mean ± s.e.m.) and BWDC (111 ± 7.6) are similar, and the ¹³C/¹²C of foliage is largely indistinguishable between sites (Supplementary Table 1), indicating similar plant-available water regimes. Atmospheric deposition contributes less than 1 kg N ha⁻¹ yr⁻¹ (ref. 17), whereas biological N₂-fixation inputs are estimated to be about 5 kg ha⁻¹ yr⁻¹, on the basis of measurements from similar mature forests in western Oregon¹⁸, empirical models¹⁹ and numerical simulations³.

In contrast, the mean N content of bedrock differs substantially: 682 ± 50 and 55 ± 6 mg N kg⁻¹ (mean ± s.e.m.) at SFM and BWDC, respectively (Fig. 1a). The bulk-N content of the SFM rock is similar to the global average for marine pelagic sediments, but is lower than for most organic-rich marine sediments, which commonly exceed 1,000 mg N kg⁻¹ (ref. 20). The differences in rock N pools translate to profoundly different N cycles: surface mineral soils in SFM forests

Table 1 | State factors and soil characteristics for forests on SFM and BWDC

Parameter	SFM	BWDC
State factors		
Parent material	Mica schist	Diorite-gabbro
Elevation (m)	1,650–1,720	1,400–1,500
Aspect	N-NE	N-NE
Precipitation (mm)	1,520	1,400
Mean annual temperature (°C)	9	10
Dominant soil type	Dystrochrept	Dystrochrept
Mineral soil characteristics (0–30 cm)		
Soil texture	Loam-sandy loam	Sandy loam
Soil pH (1:1 soil/water paste)	4.85	5.62
Bulk density (g cm ⁻³)	1.05	1.09
Coarse fragments (%)	25	30
Clay content (%)	8–12	5–8
Total C (mass %)	5.51 ± 0.30	3.54 ± 0.34
C/N (mol/mol)	20.8 ± 1.0	29.5 ± 1.3
Soil C storage (Mg ha ⁻¹)	130.2 ± 7.1	81.0 ± 7.8
Soil N storage (Mg ha ⁻¹)	7.3 ± 0.35	3.2 ± 0.26

Soil physical and chemical characteristics in the top 30 cm of mineral soil are reported. C and N pools in soil are reported as means ± s.e.m. (n = 34).

¹Department of Land, Air and Water Resources, University of California – Davis, California 95616, USA.

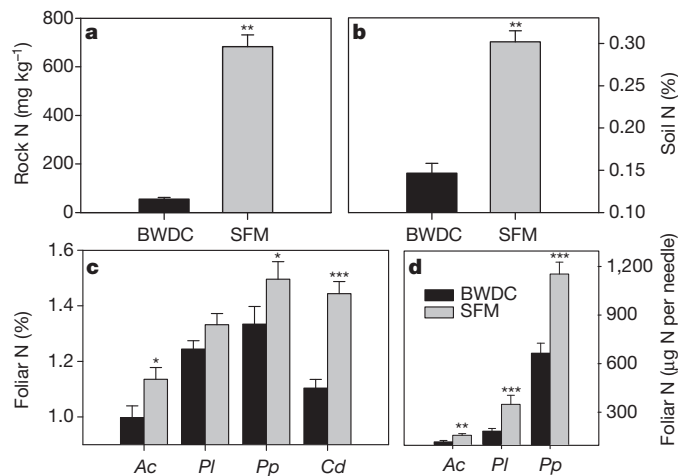


Figure 1 | Total nitrogen in rock, soil and foliage pools for SFM and BWDC forests. **a–c**, Total nitrogen in rock (mg N kg^{-1} , $n = 18$) (**a**), soil ($\% \text{N}$, $n = 34$) (**b**) and plant foliage ($\% \text{N}$, $n = 80$) (**c**) in the BWDC (black) and SFM (grey) forests. **d**, Foliar nitrogen expressed in $\mu\text{g N}$ per needle, to account for biomass dilution. *Calocedrus decurrens* is not presented in **d** because of scale-leaf rather than needle-leaf morphology. Error bars represent s.e.m. Species sampled: *Ac*, *Abies concolor*; *Pl*, *Pinus lambertiana*; *Pp*, *Pinus ponderosa*; *Cd*, *Calocedrus decurrens*. Asterisk, $P < 0.05$; two asterisks, $P < 0.01$; three asterisks, $P < 0.001$.

contain significantly more N than those in BWDC forests ($3,026 \pm 149$ and $1,426 \pm 113 \text{ mg N kg}^{-1}$ (mean \pm s.e.m.), respectively; Fig. 1b). In addition, soil C/N ratios in the top 30 cm of mineral soil are significantly lower at SFM (20.8 mol:mol) than at BWDC (29.5). Elevated total C concentrations in SFM soil result in substantially more C storage in the top 30 cm of soil at SFM ($130 \pm 7 \text{ Mg C ha}^{-1}$; mean \pm s.e.m.) than in BWDC ($81 \pm 8 \text{ Mg C ha}^{-1}$; Table 1). These differences are consistent with a California statewide soils database ($n = 183$; Supplementary Fig. 2); C and N storage at BWDC is similar to the state average for comparable ecosystems ($74.9 \text{ Mg C ha}^{-1}$, $3.89 \text{ Mg N ha}^{-1}$), whereas SFM has among the highest C and N contents observed.

Further, N enrichment in rocks and soils is readily apparent in the tree foliage. On average, conifer needles at SFM contain 50% more N per needle than at BWDC; this difference is observed in three of four sampled species (Fig. 1c); trees on SFM contain 7–30% more N on a foliar mass basis. *Calocedrus decurrens* was the most N-enriched: $1.45 \pm 0.04\% \text{ N}$ (mean \pm s.e.m.) at SFM, versus $1.10 \pm 0.03\% \text{ N}$ at BWDC. The other trees showed similar but less substantial N enrichment (*Abies concolor*, $1.14 \pm 0.04\% \text{ N}$ and $1.00 \pm 0.04\% \text{ N}$; *Pinus ponderosa*, $1.50 \pm 0.06\% \text{ N}$ and $1.33 \pm 0.06\% \text{ N}$; *Pinus lambertiana*, $1.33 \pm 0.04\% \text{ N}$ and $1.25 \pm 0.03\% \text{ N}$ at SFM and BWDC, respectively).

Under N-rich conditions, plants can either concentrate N in foliage (for example, *Calocedrus*) or build more foliage (or do both; for example *Abies* and *Pinus*), the former leading to higher N concentrations in foliage, the latter to no major changes in N contents. At SFM, needle biomass in pines is roughly 70% higher than at BWDC (Supplementary Table 2), implying significant gains in biomass with added N. Examining N contents on a per-needle basis to account for nutrient dilution²¹ reveals even more profound differences between sites: SFM trees show 35–90% more N than those at BWDC (Fig. 1d). It therefore seems that forest responses to geological N inputs are manifested as higher foliar biomass production, in addition to the higher foliar N concentrations observed.

Next, we used natural-abundance $^{15}\text{N}/^{14}\text{N}$ stable isotopes ($\delta^{15}\text{N}$ parts per thousand (‰) versus air) to trace the movement of N from rocks to soils and plants (Fig. 2). Nitrogen-isotope data for the BWDC site are consistent with expectations for other similar N-limited temperate conifer forests^{22,23}: foliar $\delta^{15}\text{N}$ ($-1.59 \pm 0.19\text{‰}$; mean \pm s.e.m.) is depleted relative to soil ($1.96 \pm 0.32\text{‰}$), whereas $\delta^{15}\text{N}$ in rocks ($18.37 \pm 1.55\text{‰}$) is substantially elevated compared with that in plants

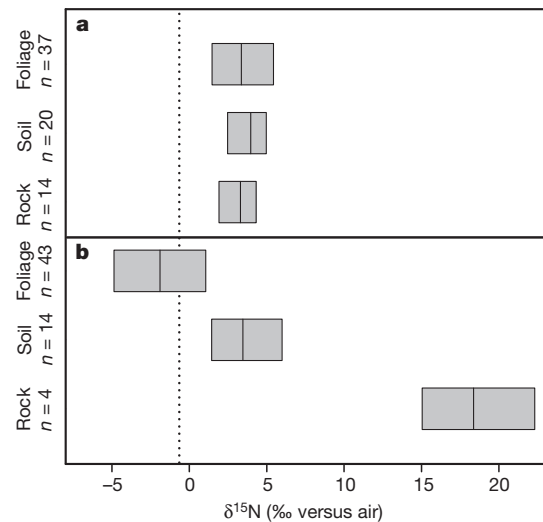


Figure 2 | Nitrogen isotope values of the rock–soil–plant system. **a**, SFM forest; **b**, BWDC forest. The median and range are plotted for each component. The dashed line represents the approximate isotope value for total atmospheric N inputs.

and soils. In contrast, foliar $\delta^{15}\text{N}$ at SFM ($3.10 \pm 0.17\text{‰}$) is 4.7‰ higher than at BWDC and is essentially indistinguishable from that of soils ($3.6 \pm 0.17\text{‰}$) and rock ($3.3 \pm 0.22\text{‰}$). This points to a direct link between weathering of rock N and the elevated N status of SFM, and conforms with general patterns of plant and soil $\delta^{15}\text{N}$ in N-rich ecosystems²³. Moreover, the lack of differentiation between the $^{15}\text{N}/^{14}\text{N}$ of rock inputs and soils at SFM indicates little or no isotopic expression through N losses at SFM. This agrees with observations of high-nitrate leachates in soils¹⁴ and streams¹² associated with N-rich rock substrates, given that N leaching does not seem to impart a major fractionation of N isotopes in comparison with gaseous losses of N (ref. 24). Finally, the contrast of plant and soil $\delta^{15}\text{N}$ pools at SFM and BWDC is consistent with models that show increased isotopic expression of ectomycorrhizal N transfer under low availability of N (ref. 25) (that is, at BWDC), although we do not observe differences in foliar $\delta^{15}\text{N}$ between ectomycorrhizal and arbuscular mycorrhizal species at either site (Supplementary Fig. 3).

Rising levels of atmospheric CO_2 and climate change have renewed interests in links between N and C cycles, especially in high-latitude forests⁴. Nitrogen limitation of extra-tropical forests is widespread²⁶; new N inputs therefore have the potential to allow for more CO_2 uptake and storage on land²⁷, thus affecting the pace and magnitude of global climate change. Using FIA data from forests developing on bedrock similar to that at SFM (eastern Franciscan, N-rich) and BWDC (western Klamath, N-poor) geological provinces of Northwest California, we show that geological N may also contribute to enhanced forest productivity and C storage on land.

Holding other state factors constant, our analysis suggests that forests on bedrock with high N-enrichment potentials (metapelites formed under a low geothermal gradient), on and within the SFM region, contain 42% more C in above-ground tree biomass than similar forests in the region that are underlain by N-depleted bedrock ($P = 0.009$, $R^2 = 0.66$; Fig. 3). Although lithology in our model represents the sum of the parent material influences on tree C stocks, the physical properties inherited from parent material, such as soil texture and depth, are taken into account by the available water-holding capacity parameter ($P = 0.001$). This implies that the enhanced C storage on putatively N-rich lithology is most associated with differences in nutrient release from rocks. Given the N-limited propensity of such forests, these region-wide results indicate higher productivity and C storage owing to bedrock N, which is consistent with the higher N and C stocks at SFM (Table 1 and Fig. 1) and with Forest Service data suggesting that

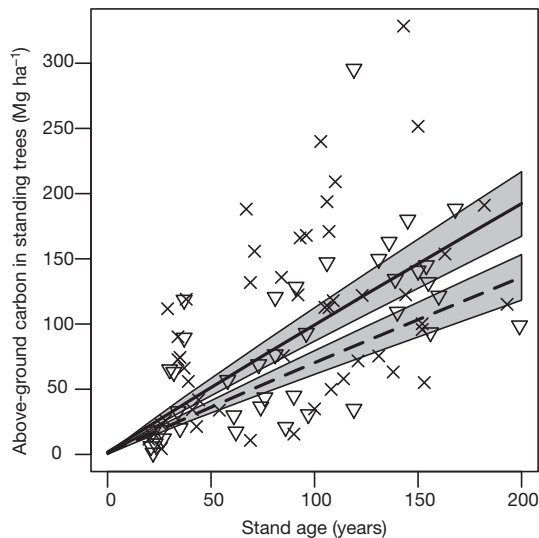


Figure 3 | Carbon in above-ground tree biomass for forests growing on N-rich and N-poor lithology. Plot of carbon (Mg ha^{-1}) against stand age for FIA plots ($n = 88$) on N-rich (crosses) and N-poor (triangles) lithologies used in the model. To account for model axes not shown, we present detransformed model estimates for sites on N-rich (solid line) and N-poor (dashed line) lithologies, holding other model parameters constant at nominal values to illustrate differences in carbon storage attributable to lithology. The grey area indicates lithology s.e.m. Our analysis estimates that sites on N-rich lithology contain 42% more C in above-ground tree biomass than sites on N-poor lithology ($P = 0.009$; adjusted $R^2 = 0.66$) after accounting for confounding state factors.

SFM contains the most productive Douglas fir forests remaining in California²⁸.

Our results raise the possibility that rock weathering may be a significant source of N to terrestrial ecosystems underlain by N-rich substrates elsewhere. There are many documented cases in which the N budgets of forests are out of balance, often being in need of substantially higher N input rates to account for N accumulation in soil and plants²⁹. In cases where bedrock is enriched in N, parent-material N could explain some (or all) of the missing N inputs. For example, using the N isotope data to devise a set of mass balance models, we estimate that rock N sources contribute 30–100% of the ecosystem N inputs at SFM, depending on the degree of isotopic expression by N losses (Supplementary Table 3). These results are comparable to simple uplift models (rock N = 47% of N inputs) and weathering experiments in the laboratory (rock N = 64% of N inputs). In terms of fluxes, these various approaches point to substantial N inputs: 3.0–10.9 $\text{kg ha}^{-1} \text{yr}^{-1}$ by rock weathering at SFM, potentially more than doubling known inputs from the atmosphere (that is, fixation plus deposition equal to 6 $\text{kg N ha}^{-1} \text{yr}^{-1}$ (refs 3, 17–19)). Given that sedimentary and metasedimentary rocks contain 99% of the global fixed N and cover roughly 75% of the Earth's land surface³⁰, the potential for bedrock N to stimulate productivity and C storage in the terrestrial biosphere seems globally significant.

METHODS SUMMARY

One-year-old sun foliage from the mid-canopy of mature conifer trees was collected with a pole saw in autumn 2008, after full needle elongation. Foliage was rinsed with deionized water and dried at 50 °C for 48 h. Needle biomass was determined by a 100-needle count on dried foliage. Samples were ground and analysed for total C and N, $\delta^{15}\text{N}$ and $\delta^{13}\text{C}$ by the University of California – Davis Stable Isotope Facility with a SerCon Hydra 20/20 isotope ratio mass spectrometer (IRMS). Isotope values are reported in parts per thousand (‰) relative to Vienna PeeDee Belemnite for $^{13}\text{C}/^{12}\text{C}$, and air N_2 for $^{15}\text{N}/^{14}\text{N}$, using standard delta (δ) notation. Surface mineral soils were collected to a depth of 30 cm, dried in air, sieved to 2 mm, milled to pass a 200- μm sieve, and then analysed by IRMS for total C and N, $\delta^{15}\text{N}$ and $\delta^{13}\text{C}$. Bulk density was determined by the core method, and soil texture by laser diffraction. Minimally weathered bedrock samples were collected

from outcrops at each site, cut with a slab saw to remove weathered surfaces, treated with 5% hydrogen peroxide for 24 h to remove any remnant surficial organic matter, and pulverized with a carbide-steel shatter box to pass a 75- μm sieve. Samples were analysed by IRMS for total C and N, $\delta^{15}\text{N}$ and $\delta^{13}\text{C}$. FIA plot data, including intensification plots, were obtained from the United States Forest Service. Above-ground carbon stocks were calculated with the Jenkins equations in the 'Fire and fuels extension' of the Forest Vegetation Simulator. Student's t -tests were used to compare differences between sites in total N in rocks, soil and foliage. The FIA model took the form of a multiple linear regression. Statistical tests and model fitting were performed in R.

Full Methods and any associated references are available in the online version of the paper at www.nature.com/nature.

Received 30 March; accepted 4 August 2011.

- Vitousek, P. M. & Howarth, R. W. Nitrogen limitation on land and in the sea: how can it occur? *Biogeochemistry* **13**, 87–115 (1991).
- Oren, R. *et al.* Soil fertility limits carbon sequestration by forest ecosystems in a CO_2 -enriched atmosphere. *Nature* **411**, 469–472 (2001).
- Wang, Y. P. & Houlton, B. Z. Nitrogen constraints on terrestrial carbon uptake: implications for the global carbon–climate feedback. *Geophys. Res. Lett.* **36**, L24403, doi:10.1029/2009gl041009 (2009).
- Magnani, F. *et al.* The human footprint in the carbon cycle of temperate and boreal forests. *Nature* **447**, 848–850 (2007).
- Galloway, J. N. in *Treatise on Geochemistry* Vol. 8 (ed. W. H. Schlesinger) 557–583 (Elsevier Pergamon, 2004).
- Holloway, J. M. & Dahlgren, R. A. Nitrogen in rock: occurrences and biogeochemical implications. *Glob. Biogeochem. Cycles* **16**, 1118, doi:10.1029/2002gb001862 (2002).
- Walvoord, M. A. *et al.* A reservoir of nitrate beneath desert soils. *Science* **302**, 1021–1024 (2003).
- Stevenson, F. J. On the presence of fixed ammonium in rocks. *Science* **130**, 221–222 (1959).
- Cornwell, S. M. & Stone, E. L. Availability of nitrogen to plants in acid coal mine spoils. *Nature* **217**, 768–769 (1968).
- Walker, T. W. & Syers, J. K. The fate of phosphorus during pedogenesis. *Geoderma* **15**, 1–19 (1976).
- Strathouse, S. M., Sposito, G., Sullivan, P. J. & Lund, L. J. Geologic nitrogen—a potential geochemical hazard in the San Joaquin Valley, California. *J. Environ. Qual.* **9**, 54–60 (1980).
- Holloway, J. M., Dahlgren, R. A., Hansen, B. & Casey, W. H. Contribution of bedrock nitrogen to high nitrate concentrations in stream water. *Nature* **395**, 785–788 (1998).
- Irwin, W., Wolfe, E. W., Blake, M. C. & Cunningham, C. G. *Geologic map of the Pickett Peak quadrangle, Trinity County, California* (US Geological Survey Map GQ-1111, 1974).
- Dahlgren, R. A. Soil acidification and nitrogen saturation from weathering of ammonium-bearing rock. *Nature* **368**, 838–841 (1994).
- Aalto, K. R. in *Geological Studies in the Klamath Mountains Province, California and Oregon. A Volume in Honor of William P. Irwin* (eds Snoke, A. W. & Barnes, C. G.) 451–464 (Geological Society of America Special Papers, vol. 410, 2006).
- Capo, R. C., Stewart, B. W. & Chadwick, O. A. Strontium isotopes as tracers of ecosystem processes: theory and methods. *Geoderma* **82**, 197–225 (1998).
- National Atmospheric Deposition Program. *National Atmospheric Deposition Program 2008 Annual Summary* (NADP Data Report 2009–01) (Univ. of Illinois at Urbana-Champaign, 2009).
- Sollins, P., Grier, C. C., McCorison, F. M., Cromack, K. & Fogel, R. The internal element cycles of an old-growth Douglas-fir ecosystem in western Oregon. *Ecol. Monogr.* **50**, 261–285 (1980).
- Cleveland, C. C. *et al.* Global patterns of terrestrial biological nitrogen (N_2) fixation in natural ecosystems. *Glob. Biogeochem. Cycles* **13**, 623–645 (1999).
- Li, Y. H. Distribution patterns of the elements in the ocean—a synthesis. *Geochim. Cosmochim. Acta* **55**, 3223–3240 (1991).
- Timmer, V. R. & Stone, E. L. Comparative foliar analysis of young Balsam fir fertilized with nitrogen, phosphorus, potassium, and lime. *Soil Sci. Soc. Am. J.* **42**, 125–130 (1978).
- Amundson, R. *et al.* Global patterns of the isotopic composition of soil and plant nitrogen. *Glob. Biogeochem. Cycles* **17**, 10.1029/2002gb001903 (2003).
- Martinelli, L. A. *et al.* Nitrogen stable isotopic composition of leaves and soil: tropical versus temperate forests. *Biogeochemistry* **46**, 45–65 (1999).
- Houlton, B. Z. & Bai, E. Imprint of denitrifying bacteria on the global terrestrial biosphere. *Proc. Natl Acad. Sci. USA* **106**, 21713–21716 (2009).
- Hobbie, E. A., Macko, S. A. & Williams, M. Correlations between foliar delta N-15 and nitrogen concentrations may indicate plant–mycorrhizal interactions. *Oecologia* **122**, 273–283 (2000).
- LeBauer, D. S. & Treseder, K. K. Nitrogen limitation of net primary productivity in terrestrial ecosystems is globally distributed. *Ecology* **89**, 371–379 (2008).
- Thomas, R. Q., Canham, C. D., Weathers, K. C. & Goodale, C. L. Increased tree carbon storage in response to nitrogen deposition in the US. *Nature Geosci.* **3**, 13–17 (2010).
- Keeler-Wolf, T. *Ecological surveys of Forest Service Research Natural Areas in California* (Gen. Tech. Rep. PSW-125) (Pacific Southwest Research Station, Forest Service, 1990).

29. Galloway, J. N., Schlesinger, W. H., Levy, H. II, Michaels, A. & Schnoor, J. L. Nitrogen fixation: anthropogenic enhancement–environmental response. *Glob. Biogeochem. Cycles* **9**, 235–252 (1995).
30. Blatt, H. & Jones, R. L. Proportions of exposed igneous, metamorphic, and sedimentary rocks. *Geol. Soc. Am. Bull.* **86**, 1085–1088 (1975).

Supplementary Information is linked to the online version of the paper at www.nature.com/nature.

Acknowledgements We thank the United States Forest Service (USFS) for access and insight, particularly D. Young and B. Rust of the Shasta-Trinity National Forest; C. Ramirez, C. Clark and D. Beardsley of USFS Region 5 Remote Sensing Office; and M. North of the Pacific Southwest Research Station for discussion of FIA modelling. I. Fisher, E. Hendel, K. Mayfield and S. Prentice assisted with sample preparation and fieldwork, and E. Brown assisted in processing strontium isotope samples. D. Beaudette

provided assistance in analysing soil data. This work was supported by grants from the David and Lucile Packard Foundation (to B.Z.H. and R.A.D.) the Andrew W. Mellon Foundation (to B.Z.H.) and the Kearney Foundation of Soil Science (to R.A.D.).

Author Contributions S.L.M., B.Z.H. and R.A.D. contributed to the experimental design and collection of field samples. S.L.M. performed sample processing and laboratory analysis. S.L.M. designed and implemented the FIA modelling component. S.L.M., B.Z.H. and R.A.D. contributed to the interpretation of laboratory data, modelling results and manuscript preparation.

Author Information Reprints and permissions information is available at www.nature.com/reprints. The authors declare no competing financial interests. Readers are welcome to comment on the online version of this article at www.nature.com/nature. Correspondence and requests for materials should be addressed to S.L.M. (slmorford@ucdavis.edu).

METHODS

Field sampling and laboratory analysis. Sampling areas were located near 40° 18' N 123° 18' W and 40° 26' N 123° 21' W for the SFM and BWDC sites, respectively. Within each sampling area, three locations were chosen at random for collection of foliage, soils and rock. A pole saw was used to collect sun needles from 10 m above the forest floor from co-dominant conifer trees in the autumn of 2008. Three clippings from each tree were bulked into a single sample. One-year-old needles were removed from the branches by hand, and needles showing damage, discoloration or herbivory were discarded. The separated needles were washed with deionized water and then dried for 48 h at 50 °C. A subsample of dried foliage was ground with a Wiley mill and then pulverized with a ball mill before chemical analysis. From the remaining sample, 100 needles were chosen at random and weighed to determine a 100-needle mass.

Ground samples were placed into tin capsules and analysed for total C and N, $^{13}\text{C}/^{12}\text{C}$ and $^{15}\text{N}/^{14}\text{N}$ on a Sercon 20/20 elemental analysis-IRMS at the University of California – Davis Stable Isotope Facility. Isotope values are reported in parts per thousand (‰) relative to Vienna PeeDee Belemnite for $^{13}\text{C}/^{12}\text{C}$ and air N_2 for $^{15}\text{N}/^{14}\text{N}$, using standard delta (δ) notation³¹. Foliage replicates had standard deviations for total C, total N, $\delta^{13}\text{C}$ and $\delta^{15}\text{N}$ of less than 0.1%, 0.05%, 0.05‰ and 0.2‰, respectively.

We dug three 50 cm × 50 cm pits in each sampling location down to the C_1 horizon (60–80 cm) to describe soil taxonomy. Additional smaller pits (0.3 m × 0.3 m) were used to collect representative mineral soil samples for the top 30 cm of the profile for chemical analysis. Soil bulk density and volume of coarse fragments were quantified in the surface mineral horizons with the use of the core method³². Soil texture was determined by laser diffraction³³. Soils were air-dried in the laboratory and sieved to 2 mm; fine roots were then removed with forceps. The soil fine fraction was ground with a ball mill, weighed into tin capsules and analysed for elemental and isotopic analysis (see foliar methods for details). Soil replicates had standard deviations for total C, total N and $\delta^{15}\text{N}$ of less than 0.02%, 0.005% and 0.3‰, respectively.

Rock samples were recovered from minimally weathered outcrops with a crack hammer. The weathering rind was removed with a lapidary slab saw. The sample was then treated with 5% hydrogen peroxide solution for 24 h to remove surficial organic matter, dried and then crushed with a hydraulic press to obtain particles with diameters of less than 10 mm. Samples were then washed with deionized water and dried at 110 °C for 48 h. A 60 g subsample was pulverized with a carbide-steel shatter box to pass a standard US 200 mesh (74- μm) sieve. Samples were weighed into tin capsules and submitted to the Stable Isotope Facility for elemental and isotopic analysis. Replicates for SFM schist had standard deviations for total N and $\delta^{15}\text{N}$ of 10 mg kg⁻¹ and 0.3‰, respectively. Replicates for rock samples from the BWDC site had higher analytical uncertainty, with standard deviations of total N of 15 mg kg⁻¹ and a $\delta^{15}\text{N}$ of 2‰. In addition, two independent methods were used to quantify total N in a subset of samples: vanadium oxide catalysed combustion³⁴ and HF/HCl digestion followed by conductimetric NH_4 quantification³⁵. Both methods resulted in N recovery within 10% of the standard elemental analysis-IRMS method.

Comparison of sample means of total N in rock, soil, and foliage between SFM and BWDC sites was performed with Student's *t*-test in R³⁶. Homogeneity of variance was tested with the Shapiro-Wilk test for normality.

For Sr analysis, rock and foliage samples were prepared as described above; 0.25 g of foliage was digested with ultrapure nitric acid and hydrogen peroxide in a CEM MDS-2100 microwave digester. Snow was collected immediately after a storm in March 2009 and passed through pre-rinsed 0.45- μm Millipore Millix syringe filters. Sr extractions for all samples were performed with Eichrom Sr-Spec resin and analysed on the Nu Plasma HR multi collector-inductively coupled plasma-mass spectrometer (MC-ICP-MS) at the University of California – Davis Interdisciplinary Center for Plasma Mass Spectrometry. Sr was corrected to $^{86}\text{Sr}/^{88}\text{Sr} = 0.1194$ to account for instrumental mass fractionation, and then normalized to SRM 987 ($^{87}\text{Sr}/^{86}\text{Sr} = 0.710248$). The SRM 987 standard averaged $^{87}\text{Sr}/^{86}\text{Sr} = 0.710269 \pm 0.000040$ (2 s.d., $n = 25$). Method blanks were less than 0.4 and 1.3 ng for rock and foliage, respectively.

Analysis of FIA plot data. A total of 130 FIA plots were identified within the designated study area and included both the standard and intensification plots for rare forest types^{37–39}. Potential N-bearing lithologies were identified with available geological data^{13,40–45}, field observations and geochemistry data from our rock collection. Potential N-rich sites occur on metasediments (blueschist facies) in the eastern Franciscan belt, whereas N-poor sites are located in terranes of western Klamath that have undergone substantial contact metamorphism. Of the 130 sites, 89 were initially selected for inclusion in the analysis by using the following criteria:

1. We selected for mixed pine, Douglas fir, Douglas fir–white fir, and Douglas fir–ponderosa pine forest types by using CalVeg classification data⁴⁶.

2. Plots occurring on ultramafic/serpentine soils were excluded by using spatial data from the Trinity serpentine soil survey⁴⁷.

3. Plots were located on slopes less than 80% and had mean annual precipitation values from 1,000 to 2,000 mm.

4. Plots had a mean stand age (defined below) of more than 20 years and less than 200 years.

5. The Stand Visualization System (SVS)⁴⁸ was used to prescreen for stands that exhibited significant mortality in the largest diameter classes resulting from extreme disturbance events such as high-intensity wildfires or insect and microbial pathogens. Stands in which more than 75% of the canopy area was occupied by dead standing trees in combination with 50–80% mortality in the largest tree diameter classes were removed from the analysis.

A total of 88 plots were included in the final analysis (Supplementary Table 4); one was removed after an analysis of disturbance regimes using fire history and stand density characteristics (discussed below).

Seven parameters were used as potential explanatory variables for the analysis. Supplementary Table 5 provides information on the central tendency and data distribution for each parameter. Non-significant variables ($P > 0.05$) were dropped from the final analysis during model fitting (see discussion below). The full set of independent parameters tested in the analysis includes:

1. Stand age. The FIA intensification plot database does not include information on stand age; we therefore estimated stand age (A_s) using a basal area-weighted function of measured conifer trees within each plot, calculated from

$$A_s = \frac{\sum A_i A_b}{\sum A_b} \quad (1)$$

where A_i is the age of an individual measured tree, and A_b is a calculated value representing the basal area per hectare. Age data from live, measured conifer trees only were only used in this determination.

2. Slope. Percentage slope was taken directly from the FIA database and converted to decimal fractions. In the case of a split plot, the mean slope across the four subplots was used.

3. Available water-holding capacity (AWHC). An estimate of the total amount of water the soil profile can hold, based on soil texture, depth and coarse fragments (fraction larger than 2 mm in diameter). AWHC values are spatially averaged values of SSURGO and STATSGO data, using a 1-km² grid⁴⁹.

4. Insolation. Annual solar input (W h m^{-2}) was derived from the 1/3-arcsecond (10-m) National Elevation Data set (NED)⁵⁰ using the Solar Analyst function⁵¹ in ArcGIS 9.3 (ref. 52). Insolation values were linearly rescaled from 0 to 1.

5. Precipitation. Mean annual precipitation was derived from the PRISM 30-arcsecond (800-m) data set (1971–2000)⁵³.

6. Temperature. Mean annual temperature was derived from the PRISM 30-arcsecond (800-m) data set (1971–2000)⁵⁴.

7. Lithology. Categorical variable that indicates whether the plot is located on lithologies with nitrogen statuses similar to SFM (eastern Franciscan) or BWDC (western Klamath).

The response variable in the model was above-ground carbon (C_a) in standing live trees (Mg C ha^{-1}). C_a was calculated on a per-tree basis by using Jenkins allometric biomass equations⁵⁵ in the 'Fire and fuels' extension⁵⁶ of the Forest Vegetation Simulator (FVS)⁵⁷.

To account for potential differences in disturbance regimes between regions, we used fire history⁵⁸ in combination with stand density information to identify plots where disturbance had substantially influenced carbon storage. A total of 26 of the initial 89 plots had a record of fire since 1920 (29%), with 11 recorded incidents in the eastern Franciscan and 15 in the western Klamath. Only 14 of the 26 fires occurred within the past 50 years, with 40% occurring in the eastern Franciscan. Inclusion of a categorical parameter in the model to account for the presence or absence of fire was non-significant ($P > 0.05$) at the three timescales examined (15, 30 and 50 years).

We compared stand density with basal area across plots to identify sites where fire significantly altered stand structure. To compare sites directly, we calculated Reineke's stand density index (SDI)⁵⁹ for each plot to account for the negative exponential relationship (reverse J-shaped distribution) between tree size and density⁶⁰. After a log-log transformation to account for data heteroscedasticity, we found a strong linear relationship between $\log(\text{SDI})$ and $\log C_a$ across lithologies and fire histories ($R^2 = 0.92$; Supplementary Fig. 4). We identified and removed a single plot that deviated significantly from the population $\text{SDI}:A_b$ trend. The removed plot, located in the western Klamath (N-poor lithology), was 194 years old with only 59 Mg C ha^{-1} in above-ground tree biomass.

We used R³⁶ to fit a multiple linear regression model, accounting for two-way interactions between local state factors. Initial model parameter selection was performed with the 'step' function in R—an implementation of Akaike's information criterion⁶¹. In favour of parsimony, the final model included only parameters

deemed significant ($P \leq 0.05$) by type II analysis of variance with the 'Anova' function from the Companion to Applied Regression (CAR)⁶² library in R³⁶. The final model took the form

$$\log C_a = \beta_0 + \log x_1 + x_2 + x_3 + x_4 + x_5 + x_6 + \varepsilon \quad (2)$$

where β_0 is the intercept, x_1 – x_6 represent coefficients fitted by the model (x_1 , stand age; x_2 , lithology, x_3 , temperature, x_4 , AWHC; x_5 , insolation; x_6 , AWHC \times insolation) and ε represents error. An ANOVA table for the final model is presented in Supplementary Table 6). Precipitation ($P = 0.12$) and slope ($P = 0.49$) were found to be non-significant in the final model. Collinearity was assessed by using the variance inflation factor from the CAR package⁶² (Supplementary Table 7). Model coefficient tables (Supplementary Table 7), model fit information (Supplementary Fig. 5) and residual plots (Supplementary Fig. 6) are also presented.

Mass balance modelling methods for determination of bedrock N flux. We developed four simple models derived from natural-abundance N isotope data, tectonic uplift rates and laboratory weathering experiments to better constrain N input fluxes from bedrock into our sites. Our first two models apply principles of isotopic mass balance: model A estimates rock N contribution to the ecosystem under the assumption of no isotopic fractionating loss, whereas model B assumes that fractionating loss pathways are similar among sites. Model C uses steady-state assumptions to estimate N inputs using rock N content, tectonic uplift rates, and chemical weathering potential. Finally, model D uses laboratory weathering experiments, corrected for temperature with Arrhenius relationships. All models were implemented in R and results are based on 100,000 Monte Carlo simulations. We report 2.5th centiles, medians and 97.5th centiles of all model outputs, representing a 95% confidence interval around our estimates.

In model A we employ a simple mixing model to estimate the fraction of rock N inputs to the ecosystems (f_{rock} , equation (3)), using measured isotopic data and estimated pool sizes. The major assumption in this model is that there is no fractionating loss at either the BWDC or SFM site. We estimate an ecosystem $^{15}\text{N}/^{14}\text{N}$ ($\delta^{15}\text{N}_{\text{ecosystem}}$) pool through the mixing of soil (f_{soil}) and biomass (f_{plant}) pools. The relative size of the soil versus biomass pools is difficult to quantify for these sites; however, we can use estimates of forest ecosystem carbon pools⁶³ and the C/N of plant biomass pools^{3,64,65} to predict a range of possible relative pool sizes. Using these constraints, we calculate that 0.07–0.40 of the ecosystem N reservoir is contained within plant biomass, but larger values most probably represent forests where soil C and N storage is low. In our model we use a range of 0.07–0.20 for the biomass contribution to the total ecosystem N pool, and assume that the $^{15}\text{N}/^{14}\text{N}$ of foliage is representative of the entire biomass pool ($\delta^{15}\text{N}_{\text{plants}}$, equation (4)). The $^{15}\text{N}/^{14}\text{N}$ of the atmospheric endmember ($\delta^{15}\text{N}_{\text{atm}}$) is assumed to range from -1.5‰ to -0.5‰ , and $^{15}\text{N}/^{14}\text{N}$ of the rock ($\delta^{15}\text{N}_{\text{rock}}$) and soil ($\delta^{15}\text{N}_{\text{soil}}$) components in the model represent the mean \pm s.e.m. for each pool.

$$f_{\text{rock}} = (\delta^{15}\text{N}_{\text{ecosystem}} - \delta^{15}\text{N}_{\text{atm}}) / (\delta^{15}\text{N}_{\text{rock}} - \delta^{15}\text{N}_{\text{atm}}) \quad (3)$$

$$\delta^{15}\text{N}_{\text{ecosystem}} = f_{\text{soil}}(\delta^{15}\text{N}_{\text{soil}}) + f_{\text{plants}}(\delta^{15}\text{N}_{\text{plants}}) \quad (4)$$

Model B differs from model A in that it incorporates a fractionating loss term whereby isotopically light N is removed preferentially from the ecosystem (equation (5)). Loss pathways include both leaching (f_{leaching}) and denitrification (f_{denit}); however, evidence indicates that the isotope effect of leaching is approximately zero when integrated through space and time²⁴ (equation (6)), leaving denitrification as the sole fractionating loss pathway in the ecosystem. To consider isotopic effects of N losses, we make two simplifying assumptions. First, we assume that the contribution of N from rock is effectively zero at the BWDC forest. Second, we assume that the relative imprint of denitrification on the total ecosystem pool is the same between sites, given the similarity of climate, vegetation and soil physical properties between SFM and BWDC. In doing so, we combine the fraction and isotope term in the denitrification pathway into a single variable, η (equation (7)). Using the assumptions from equations (6) and (7), we can solve for η (equation (8)) and the fraction of rock inputs at the SFM site (equation (9)):

$$\delta^{15}\text{N}_{\text{ecosystem}} = f_{\text{atm}}(\delta^{15}\text{N}_{\text{atm}}) + f_{\text{rock}}(\delta^{15}\text{N}_{\text{rock}}) - f_{\text{denit}}(\varepsilon_{\text{denit}}) - f_{\text{leaching}}(\varepsilon_{\text{leaching}}) \quad (5)$$

$$\varepsilon_{\text{leaching}} = 0 \quad (6)$$

$$\eta = f_{\text{denit}}(\varepsilon_{\text{denit}}) \quad (7)$$

$$\eta = \delta^{15}\text{N}_{\text{atm}} - \delta^{15}\text{N}_{\text{BWDC}} \quad (8)$$

$$\frac{\delta^{15}\text{N}_{\text{SFM}} + \eta - \delta^{15}\text{N}_{\text{atm}}}{\delta^{15}\text{N}_{\text{SFMrock}} - \delta^{15}\text{N}_{\text{atm}}} = \frac{\delta^{15}\text{N}_{\text{SFM}} - \delta^{15}\text{N}_{\text{BWDC}}}{\delta^{15}\text{N}_{\text{SFMrock}} - \delta^{15}\text{N}_{\text{atm}}} = f_{\text{rock}} \quad (9)$$

For model C we estimated the rock N contribution to SFM and BWDC ecosystems from regional uplift rates and atmospheric N inputs. We assumed that uplift equals denudation rates at our sites and that the chemical weathering fraction is between 0.05 and 0.2 of the total denudation rates, on the basis of estimates from the Sierra Nevada⁶⁶. Total atmospheric N inputs are between 4 and 8 kg ha⁻¹ yr⁻¹ at both sites, on the basis of regional estimates of N fixation^{3,17,18} and N deposition¹⁶. Quaternary uplift rates in the northwestern California are estimated to be between 0.001 and 0.004 m yr⁻¹, on the basis of geodynamic models^{67,68} and field data^{69,70}. The fraction of rock N input to the ecosystem (f_{rock}) can then be estimated from equation (10):

$$f_{\text{rock}} = r_u f_{\text{cw}} (10,000 \text{ m}^2 \text{ ha}^{-1}) \rho_d N_{\text{rock}} [1 / (1 + i_{\text{atmos}})] \quad (10)$$

where r_u is uplift rate (m yr⁻¹), f_{cw} is the chemical weathering fraction, ρ_d is rock density (kg m⁻³), N_{rock} is the N content of bedrock, and i_{atmos} is the total atmospheric N input (kg ha⁻¹ yr⁻¹).

In model D we estimate rock N inputs at SFM on the basis of laboratory weathering data⁷¹. Bulk leaching experiments estimated bedrock N fluxes to be between 5 and 38 kg⁻¹ ha⁻¹ yr⁻¹ after 360-day incubations at 20 °C. Mineral dissolution rates are sensitive to temperature^{30,72,73}; we therefore estimate field N fluxes on the basis of laboratory weathering rates corrected for differences in temperature between the laboratory (20 °C) and field (9 °C), using Arrhenius relationships. Activity coefficients for potassium are used in place of ammonium, given the similarity in charge and ionic radius of ammonium and large-ion lithophiles in geochemical systems⁷⁴. The field weathering rate (r_{field}) is estimated from equation (11):

$$r_{\text{field}} = \exp \left[\frac{-E_a}{R} \left(\frac{1}{T_{\text{field}}} - \frac{1}{T_{\text{lab}}} \right) \right] r_{\text{lab}} \quad (11)$$

where E_a is the dissolution activity energy, R is the gas constant, r_{lab} is the laboratory weathering rate, and T_{field} and T_{lab} are field and laboratory temperatures, respectively.

Methods for statewide soil C and N analysis. A total of 183 pedons from the University of California – Davis Soil library were selected for the analysis, on the basis of vegetation data (mixed conifer and Douglas fir). Soils with andic properties were identified and excluded from the analysis by using the database soil taxonomy and through comparison with SSURGO⁷⁵ soil survey data at the pedon location. The aqp⁷⁶ package in R³⁶ was used to calculate the depth-integrated C and N content for each pedon at intervals of 1 cm. Calculation of carbon and nitrogen soil storage were based on the horizon-integrated N and C content, the volume of coarse fragments, and the soil bulk density. The bulk density data from the database were incorrect or missing for several pedons; to correct for this, we assumed that bulk density increased linearly from 1,000 kg m⁻³ at the soil surface to 1,200 kg m⁻³ at 30 cm.

- McKinney, C. R., McCrea, J. M., Epstein, S., Allen, H. A. & Urey, H. C. Improvements in mass spectrometers for the measurement of small differences in isotope abundance ratios. *Rev. Sci. Instrum.* **21**, 724–730 (1950).
- Blake, G. R. & Hartge, K. H. in *Methods of Soil Analysis—Physical and Mineralogical Methods* Vol. 9 (ed. Klute, A.) Ch. 13 364–367 (Soil Science Society of America, 1986).
- Eshel, G., Levy, G. J., Mingelgrin, U. & Singer, M. J. Critical evaluation of the use of laser diffraction for particle-size distribution analysis. *Soil Sci. Soc. Am. J.* **68**, 736–743 (2004).
- Brauer, K. & Hahne, K. Methodical aspects of the N-15-analysis of Precambrian and Palaeozoic sediments rich in organic matter. *Chem. Geol.* **218**, 361–368 (2005).
- Carlson, R. M. Automated separation and conductimetric determination of ammonia and dissolved carbon dioxide. *Anal. Chem.* **50**, 1528–1531 (1978).
- R Development Core Team. *R: A Language and Environment for Statistical Computing v.2.12.1* (R Foundation for Statistical Computing, 2010).
- USDA Forest Service. *2007 Mendocino National Forest Vegetation Inventory* (Pacific Southwest Research Station, 2010).
- USDA Forest Service. *2007 Shasta–Trinity National Forest Vegetation Inventory* (Pacific Southwest Research Station, 2010).
- USDA Forest Service. *2007 Six Rivers National Forest Vegetation Inventory* (Pacific Southwest Research Station, 2010).
- Bishop, D. G. South-Fork Mountain Schist at Black-Butte and Cottonwood Creek, northern California. *Geology* **5**, 595–599 (1977).
- Jayko, A. S. & Blake, M. C. Deformation of the eastern Franciscan belt, northern California. *J. Struct. Geol.* **11**, 375–390 (1989).
- Lanphere, M. A., Blake, M. C. & Irwin, W. P. Early Cretaceous metamorphic age of South Fork Mountain Schist in northern Coast Ranges of California. *Am. J. Sci.* **278**, 798–815 (1978).

43. Jennings, C. W. & Strand, R. *Geologic Map of California: Ukiah Sheet* (California Division of Mines and Geology, 1960).
44. Strand, R. G. *Geologic Map of California: Redding Sheet* (California Division of Mines and Geology, 1962).
45. Blake, M. S., Helley, E. J., Jayko, A. S., Jones, D. L. & Ohlin, H. N. *Geologic Map of the Willows 1:100,000 Quadrangle, California* (US Geological Survey Open-File Report OF-92-271, 1992).
46. USDA Forest Service. *Existing Vegetation—CALVEG Geodatabase* (USDA Forest Service, Pacific Southwest Region Remote Sensing Lab, 2009).
47. USDA Forest Service. *Trinity Serpentine Soil Survey* (Pacific Southwest Research Station, 2004).
48. McGaughey, R. J. *Stand Visualization System v. 3.3* (United States Department of Agriculture, Forest Service, Pacific Northwest Research Station, 2004).
49. Beaudette, D. E. & O'Geen, A. T. *A 1 km Scale, Gridded Soils Database for California* (California Soil Resource Lab, Univ. of California, Davis, 2010).
50. Gesch, D. B. in *Digital Elevation Model Technologies and Applications: The DEM User Manual* 2nd edn (ed. Maune, D.) 99–118 (American Society for Photogrammetry and Remote Sensing, 2007).
51. Fu, P. & Rich, P. M. A geometric solar radiation model with applications in agriculture and forestry. *Comput. Electron. Agric.* **37**, 25–35 (2002).
52. Environmental Systems Research Group. *ArcGIS Desktop v. 9.3* (Environmental Systems Research Group, Redlands, 2010).
53. The PRISM Group at Oregon State University. *United States Average Monthly or Annual Precipitation, 1971–2000* (Oregon State Univ., 2006).
54. The PRISM Group at Oregon State University. *United States Average Monthly or Annual Maximum Temperature, 1971–2000* (Oregon State Univ., 2006).
55. Jenkins, J. C., Chojnacky, D. C., Heath, L. S. & Birdsey, R. A. National-scale biomass estimators for United States tree species. *For. Sci.* **49**, 12–35 (2003).
56. Reinhardt, E. D., Crookston, N. L. & Rebaun, S. A. *The Fire and Fuels Extension to the Forest Vegetation Simulator* (United States Department of Agriculture, Forest Service, 2003).
57. Forest Inventory and Analysis Program. *The Forest Inventory and Analysis Database: Database Description and Users Manual Version 3.0 for Phase 2, Revision 1.* (United States Department of Agriculture, Forest Service, 2008).
58. California Department of Forestry and Fire Protection. *Fire Perimeters (1923 to 2008) for Wildfire in the State of California* (State of California, 2009).
59. Reineke, L. H. Perfecting a stand-density index for even-aged forests. *J. Agric. Res.* **46**, 627–638 (1933).
60. Smith, E. M., Larson, B. C., Kelty, M. J. & Ashton, P. M. S. *The Practice of Silviculture: Applied Forest Ecology* 9th edn (Wiley, 1996).
61. Akaike, H. A new look at the statistical model identification. *IEEE Trans. Automat. Contr.* **16**, 716–723 (1974).
62. Fox, J. & Weisberg, S. *An (R) Companion to Applied Regression* (Sage, 2011).
63. Lorenz, K. & Lal, R. *Carbon Sequestration in Forest Ecosystems* (Springer, 2010).
64. de Vries, W. *et al.* Ecologically implausible carbon response? *Nature* **451**, E1–E3 (2008).
65. Townsend, A. R., Braswell, B. H., Holland, E. A. & Penner, J. E. Spatial and temporal patterns in terrestrial carbon storage due to deposition of fossil fuel nitrogen. *Ecol. Appl.* **6**, 806–814 (1996).
66. Riebe, C. S., Kirchner, J. W. & Finkel, R. C. Sharp decrease in long-term chemical weathering rates along an altitudinal transect. *Earth Planet. Sci. Lett.* **218**, 421–434 (2004).
67. Lock, J., Kelsey, H., Furlong, K. & Woolace, A. Late Neogene and Quaternary landscape evolution of the northern California Coast Ranges: evidence for Mendocino Triple Junction tectonics. *Geol. Soc. Am. Bull.* **118**, 1232–1246 10.1130/b25885.1 (2006).
68. Mitchell, C. E., Vincent, P., Weldon, R. J. & Richards, M. A. Present-day vertical deformation of the Cascadia Margin, Pacific Northwest, United States. *J. Geophys. Res. Solid Earth* **99**, 12257–12277 (1994).
69. Kelsey, H. M., Engebretson, D. C., Mitchell, C. E. & Ticknor, R. L. Topographic form of the Coast Ranges of the Cascadia Margin in relation to coastal uplift rates and plate subduction. *J. Geophys. Res. Solid Earth* **99**, 12245–12255 (1994).
70. Merritts, D. & Bull, W. B. Interpreting quaternary uplift rates at the Mendocino Triple Junction, northern California, from uplifted marine terraces. *Geology* **17**, 1020–1024 (1989).
71. Dahlgren, R. A. Geologic nitrogen as a source of soil acidity. *Soil Sci. Plant Nutr.* **51**, 719–723 (2005).
72. Casey, W. H. & Sposito, G. On the temperature-dependence of mineral dissolution rates. *Geochim. Cosmochim. Acta* **56**, 3825–3830 (1992).
73. Brady, P. V. & Carroll, S. A. Direct effects of CO₂ and temperature on silicate weathering—possible implications for climate control. *Geochim. Cosmochim. Acta* **58**, 1853–1856 (1994).
74. Verrall, R. E. Determination of activity coefficients for ammonium chloride at 25 °C. *J. Solution Chem.* **4**, 319–329 (1974).
75. Soil Survey Staff. *Soil Survey Geographic (SSURGO) Database for California* (United States Department of Agriculture, Natural Resources Conservation Service, 2010).
76. Beaudette, D. E. & O'Geen, A. T. *Algorithms for Quantitative Pedology: A Toolkit for Soil Scientists* (California Soil Resource Lab, Univ. of California, Davis, 2010).